Microfluidic Microdialysis: Spatiotemporal Control over Solution Microenvironments Using Integrated Hydrogel Membrane Microwindows

Joel S. Paustian, Rodrigo Nery Azevedo, Sean-Thomas B. Lundin, Matthew J. Gilkey, and Todd M. Squires[*]

Department of Chemical Engineering, University of California, Santa Barbara, California 93106, USA

We present a powerful and versatile technique that enables exquisite spatial and temporal control over local solution chemistry in microfluidic devices. Using a microscope and a UV lamp, we use projection lithography to photopolymerize thin (10–25 μm) hydrogel membrane "microwindows" (HMMs) into standard microfluidic devices. These microwindows are permeable to solute and solvent diffusion and to electric fields, yet act as rigid walls from the standpoint of fluid flow. Reservoirs of solution may thus be rapidly imposed, switched, and maintained on one side of a HMM using standard microfluidic techniques, provoking changes in solution conditions on the other side without active mixing, stirring, or diluting. We highlight three paradigmatic experimental capabilities enabled by HMMs: (1) rapid dialysis and swapping of solute and/or solvent, (2) stable and convection-free localized concentration gradients, and (3) local electric permeability. The functional versatility of hydrogel microwindow membranes, coupled with the ease and speed of their fabrication and integration into simple microchannels or multilayer devices, will open a variety of novel applications and studies in a broad range of fields.

Subject Areas: Interdisciplinary Physics, Materials Science, Soft Matter

I. INTRODUCTION

Provoking the response of cells, organisms, solutions, and materials to environmental changes is a nearly ubiquitous demand in biology, chemistry, physics, and materials science. Microfluidic devices enable such studies to be performed on micron scales [1–5], with precise geometric and fluidic control over small sample volumes [6,7]. Techniques for microfluidic logic [8] have enabled large-scale integration of microfluidic devices capable of complex experiments and high-throughput parameter sweeps [9]. Robust and versatile methods for sculpting local chemical environments in space and time, however, have remained elusive.

The vertebrate circulatory system provides an ideal model for the rapid and precise chemical delivery to soft targets, by using a stepwise method of convection followed by diffusion. Gas, nutrients, and other solutes are convected rapidly over large distances through arteries and vessels until they reach smaller capillaries, which are distributed densely enough that solute can diffuse rapidly across membranes or pores and into tissues and cells.

Here, we describe a powerful, versatile, yet simple element for microfluidic systems—hydrogel microwindow membranes (HMMs)—that enable an analogous stepwise convective-diffusive chemical delivery in microfluidic systems. HMMs provide an unparalleled combination of rapid delivery, spatial control, optical accessibility, simple and

[*]Corresponding author.
squires@engineering.ucsb.edu

rapid device fabrication, and integration with standard devices. HMMs are compatible with existing microfluidic materials and fabrication techniques, and they enable the rapid imposition and switching of *local* microchemical environments, without introducing convective flows near the sample that might disrupt or wash away fragile or unbound materials. Moreover, HMMs can operate scalably within complex microfluidic devices, as each HMM functions independently, without interfering with others in the network.

The core HMM strategy is illustrated in Figs. 1 and 2. A "reservoir channel" (which will contain the solution to be delivered) is made to run alongside a "sample" channel (to which the solution will be delivered), with a gap in the wall separating them. A thin (10–25-μm-wide) hydrogel membrane microwindow placed in this gap then allows local microdialysis. Its pores are small enough that it acts like an impermeable wall from the standpoint of fluid flow, yet is permeable to electric fields, solute, and solvent. A solution flowing through the reservoir channel establishes and maintains a steady reservoir of solute, which subsequently diffuses through the membrane and into the sample channel. The thinness of the membrane, and the small dimensions characteristic of microfluidic devices, renders a short time scale for diffusive delivery ($\tau_D \sim L^2/D$). Dissolved salts ($D \sim 10^3$ μm^2/s), for example, require $\tau_D \sim 100$ ms to diffuse 10 μm, and $\tau_D \sim 10$ s to diffuse 100 μm.

Several essential features are readily apparent. (1) HMMs are exceptionally thin, which enables fast diffusive delivery. (2) Microdevices can be designed with multiple microwindow membranes, each with a distinct, independently controlled reservoir channel. Almost arbitrarily complex solution microenvironments can thus be designed into microfluidic systems, e.g., with multiple components, introduced at multiple locations and/or times,
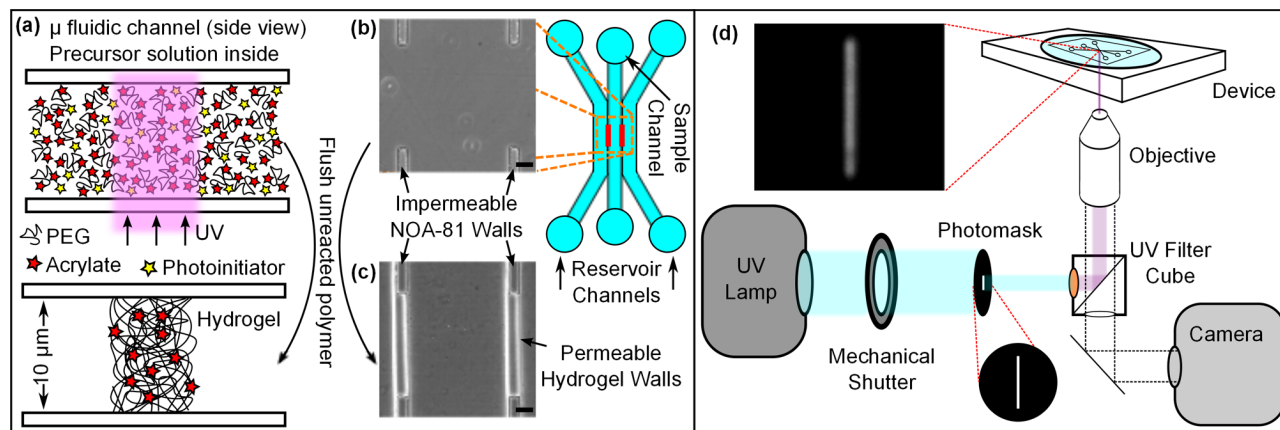
FIG. 1. Fabrication of HMMs. (a) A UV-polymerizable solution of poly(ethylene-glycol)-diacrylate and photoinitiator initially fills a three-channel microfluidic device (b), with gaps in the walls between channels. Patterned UV light is used to cross-link the hydrogel in two specified rectangular regions (width: 10–20 μm) filling the gaps in the walls. (c) After flushing the unreacted solution, hydrogel microwindow membranes remain (phase contrast, scale bar = 20 μm). (d) Simplified microscope schematic for fabricating HMMs. The microfluidic device is placed on the microscope stage, and a photomask is inserted into the microscope field aperture. A computer-controlled mechanical shutter exposes the PEG-DA solution to UV irradiation for the desired exposure time. Inset: Natural fluorescence of NOA-81 optical glue enables the patterned UV light to be aligned.

as well as sharp concentration gradients (e.g., several molar over tens of μm). (3) HMMs are permeable to electric fields, enabling localized electrokinetic effects (e.g., selective electroporation, electrophoresis, sorting, and separations) to be incorporated into complex microfluidic devices. (4) Integration with microfluidic plumbing and logic (including elastomeric valves in polydimethylsiloxane
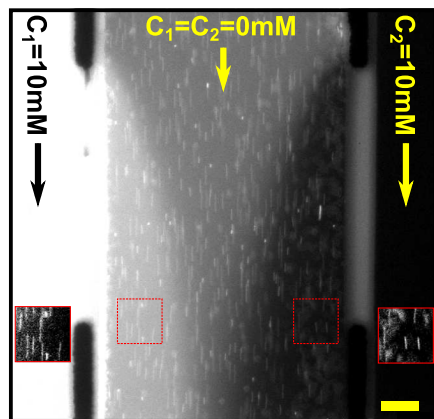

FIG. 2. (See Video 1.) HMMs are permeable to small-molecule solutes, yet admit no measurable hydrodynamic flow. Here, we use the three-channel device shown in Fig. 1(b) and specifically show the same close-up view as Fig. 1(c). All channels contain a fluorescent pH indicator at the same concentration, and each channel is buffered at a different pH: 8.1 (left, bright), 6.3 (center, intermediate), and 4.7 (right, dark), with ionic strengths balanced. Fluorescent tracer particles (bright lines) travel in straight lines past the center channel, indicating no convective inflow through either the left or right HMM. Diffusion of pH buffers through the membrane is clearly evident. Insets: Contrast-enhanced and enlarged images showing tracer particle paths. Scale bar: 20 μm.

(PDMS) devices [10]) enables rapid switching of reservoir solutions and, consequently, of the local solution chemistry within the sample chamber. (5) HMMs hydrodynamically isolate reservoir and sample channels in complex-device geometries, without requiring pressures to balance as in laminar-flow strategies. Each HMM can thus operate independently, without interfering with upstream or downstream HMMs. (6) The fabrication strategy is relatively simple, requiring little more equipment than is standard in most research laboratories. (7) HMMs do not interfere with optical access to the sample, whereas, e.g., track-etched membranes used to introduce solute to a channel from above or below [11] interfere with the optical path. Instead, sample and reservoir channels can lie entirely within a single focal plane, allowing high-resolution gradient visualization within microscale regions and improved synchronization with reservoir channel flow switching. Hydrogel microwindow membranes can be integrated into conventional microfluidic channel materials, and hydrogel chemistries can be readily adapted as needed for particular chemical demands, e.g., to be permeable to a range of solutes and solvents. We therefore anticipate that HMMs will enable a broad range of capabilities for microfluidic studies and applications that demand precise spatial and temporal control over solute and solvent distribution.

We begin with a brief discussion of existing techniques for microfluidic solution manipulation in Sec. II, then continue with a brief description of a HMM fabrication procedure in Sec. III. Section IV presents the basic operation and properties of HMMs, with Sec. IVA showing HMM functions for the flow-free introduction of solute (pH buffers, evidenced with a fluorescent pH indicator; Fig. 2) and solvent (triggering local antisolvent crystallization; Fig. 3). Section IV B details methods to measure
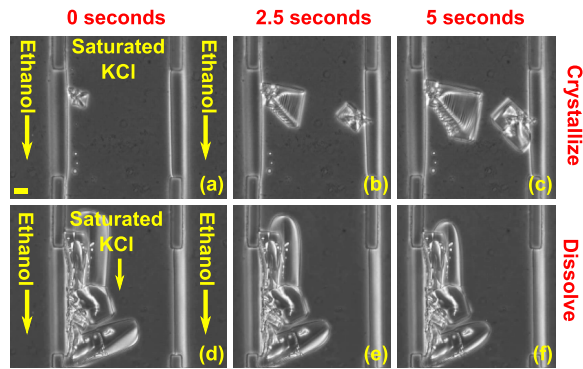
FIG. 3. Antisolvent diffuses from the reservoir channels across HMMs into a saturated aqueous salt solution in the sample channel, depicted in the three-channel device of Figs. 1(b) and 1(c). (a-c) Upon stopping KCl flow in the sample channel, ethanol diffuses through the HMMs. As ethanol concentration progressively increases near the HMM, KCl solubility decreases, triggering nucleation and growth of KCl crystals. (d-f) Resuming convective delivery of fresh aqueous KCl solution flushes away the ethanol, restoring KCl solubility to its bulk aqueous value, and dissolving the crystals. (See Videos 2 and 3.) (Phase contrast, scale bar = 20 μm.)

and control the diffusive and convective permeabilities of the microwindows. We then present paradigmatic experiments that highlight the versatility and range of capabilities afforded by HMMs. Section V shows rapid dialysis of solute and solvent, Sec. VI shows local electric permeability and field sculpting, and Sec. VII shows rapid imposition of localized concentration gradients, which enables the first direct visualization of colloidal solvophoresis [Fig. 7(c)]. Along with these demonstrations, we describe several novel methods yielded by HMMs to manipulate and visualize colloids and solutions at the microscale.

II. PREVIOUS WORK

Steady chemical gradients have been created convectively, by using T junctions [12] to bring two solutions into coflowing contact. These can be used to expose surface-fixed samples to chemical gradients or dynamic environments [13,14]. However, resulting shear may disrupt or perturb soft samples (e.g., cells or tissues, soft materials, or growing crystals), and flow itself may displace unbound samples (including material precursors, existing solutions, particles, or cells) or disrupt gradients. Although shear may be reduced using channel networks for gradient generation [15], all flow-based strategies require precise pressure balances to properly align flows [16], as well as relatively large device areas [17]. Therefore, they become increasingly impractical as devices become more complex. Coflowing techniques are well suited for certain experiments but do not represent a versatile, robust technique to rapidly introduce, controllably vary, or precisely sculpt local chemical microenvironments. Convective solution modification has also been achieved by adding ingredients sequentially, via a rotary mixer [18], enabling automated

batch preparation of solutions [19], yet each added aliquot necessarily flushes out an equal volume of the existing sample. In some cases, this flushing is advantageous—e.g., in maintaining a stable microbial population in a microchemostat [20]—but continuous dilution is undesirable in other experiments.

Introducing solute or solvent diffusively can alleviate some of the issues associated with flow, but it poses separate challenges. Diffusive transport becomes prohibitively slow over long distances: The time τ_D for a species with diffusivity D to diffuse a distance L scales like $\tau_D \sim L^2/D$, and any flow U—stray or otherwise—overwhelms this diffusive delivery beyond a critical length scale $L_c \sim D/U$. Batch diffusive mixing has been enabled through free-interface diffusion, initiated by opening PDMS valves between microchambers [21–24] or sliding lubricated substrates to bring loaded microchambers on opposite sides into contact [25–27]. Such strategies, however, cannot maintain steady gradients. Steady gradients have been produced by controllably contacting flowing source and sink solutions with large ($L \sim 1$ mm, $\tau_D \gtrsim 1000$ s) flow-free channels [28] or chambers [29], but reductions in chamber size (and τ_D) would result in increased stray convection.

Methods for embedding or fabricating membranes within microfluidic channels have employed stepwise convection-diffusion into microfluidic devices, allowing diffusive solute delivery [30,31]. Contact photolithography has been used to photopolymerize hydrogels [32] to create permeable plugs or microchamber walls [33–37]. At standard device thicknesses, contact lithography exhibits limited resolution [38], which was overcome by projecting shaped laser beams into microchannels using custom optics [38–40]. Besides photopolymerization, membrane fabrication has been achieved via interfacial polymerization [41] and evaporative assembly of packed beds [42]. Embedding opaque track-etched membranes between multiple microchannel layers [11,17,43,44] allows precise control of pore size and visualization of the bottom channel layer, while polymerization of suspended gels enables membranes in capillary-filled channels [45]. Devices made entirely of solute-permeable materials [46–49] allow diffusive delivery along entire channels. Previous works have not, however, demonstrated the *rapid* (seconds) and *localized* (20 μm) flow-free solution swapping and strong gradient generation afforded by HMMs, which exploit the rapid diffusive equilibration across thin, high-porosity hydrogel membranes.

III. MICROWINDOW FABRICATION

To make HMMs, we employ microscope projecton photolithography (MPP) [50], in which a standard microscope provides high-resolution photopatterning with UV illumination. In MPP, a photomask is placed within the field conjugate plane, usually in the microscope's field diaphragm, yielding patterned UV illumination in the focal plane. The photomask pattern is also magnified by the

objective, resulting in enhanced resolution. The technique has recently become common for flow lithography, wherein hydrogel particles are synthesized within flowing solutions of UV-curable molecules through PDMS channels [51–56]. The polymerization reaction is inhibited by oxygen that permeates through the PDMS walls, resulting in freely flowing hydrogel particles [57]. MPP has also been used to pattern 150-μm-wide gel barriers [58] and hydrogel posts [59] on glass surfaces in glass/PDMS channels.

Using MPP, we pattern the photopolymerization of poly (ethylene-glycol)-diacrylate (PEG-DA) precursor solutions to form hydrogel membranes that are much thinner than would be possible using standard methods such as contact lithography. (See Fig. 1 and Appendix A 1 for experimental details.) Owing to its versatile chemistry, PEG-DA has been widely used in continuous-flow lithography (e.g., [52]) and in gel-based microfluidic devices (e.g., [47]). We focus on the fabrication, operation, and capabilities of HMMs polymerized into devices made from microfluidic ''stickers'' (Norland Optical Adhesives, NOA-81, thiol-ene–based photopolymer) [60], which we found to be straightforward because of the fast templating, oxygen impermeability, and reactivity [61] of these microchannels. We have also developed techniques for fabricating HMMs in PDMS channels through surface modifications, which will be described in a later work. Either device type can be integrated with PDMS microvalves, if desired, to achieve precise flow control and rapid switching (e.g., Fig. 5).

IV. OPERATION AND PROPERTIES

A. Solution sculpting

For HMMs to function appropriately, they must be permeable to the diffusive transport of solute and solvent, yet concurrently act as rigid, impermeable walls from the standpoint of fluid flow. These twin demands require a hydrogel that is chemically inert, with pores that are large enough to admit molecular diffusion, yet small enough to prevent appreciable flow.

Figure 2 and related Video 1 demonstrate the successful operation of HMMs. Each of the three channels contains 25 μM fluorescein, which functions as a pH indicator because of its increasing fluorescence intensity between pH 5 and 9. Solutions buffered at different pH are driven through the three channels: The left (reservoir) channel is maintained at pH 8.1 by a 10-mM tris buffer and appears bright; the right (reservoir) is held at pH 4.7 by a 10-mM acetate buffer and appears dark; and the center (sample) channel is held at pH 6.3 by a 1-mM 2-(N-morpholino)ethanesulfonic acid (MES) buffer along with 9-mM KCl to balance ionic strength, and it appears grey. Fluorescent polystyrene beads are also present in the center solution and serve as flow tracers (Bangs Labs FS03F, 500nm, 0.02wt%). All channel outlets were connected to a waste reservoir, the two reservoir channel inlets were pressurized at 150 mbar using compressed air, and the sample channel inlet was held at 2 mbar with hydrostatic

pressure, giving a transmembrane pressure $\Delta P_m = 75$ mbar and flow velocities that are 75 times faster in reservoir channels than in the sample channel. Buffers in the reservoir channels visibly diffuse into the sample channel, as indicated by the change in fluorescence intensity, and are convected downstream by the sample channel flow. Tracer particles in the sample channel follow straight trajectories past the HMMs, indicating the absence of detectable hydrodynamic flow through the membrane, despite the trans-HMM pressure difference. Transport of buffer through the HMM from the reservoir to the channel is thus predominantly diffusive.

HMMs are also permeable to solvents that are miscible with water, allowing solvent, as well as solute, to be introduced from reservoirs. Ethanol, for example, reduces the solubility of KCl in water and can be delivered through HMMs to trigger antisolvent crystallization. Figure 3 shows a three-channel device, where ethanol flows through the two outer reservoir channels, and saturated KCl flows through the central sample channel. When the KCl flow stops [Fig. 3(a)], ethanol diffuses into the quiescent KCl solution in the sample channel, provoking the nucleation and growth of salt crystals [Figs. 3(b) and 3(c) and related Video 2]. Flushing the antisolvent by restarting KCl flow [Fig. 3(d)] causes the KCl crystals to gradually dissolve [Figs. 3(e) and 3(f) and related Video 3]. Such crystallization-dissolution experiments can be repeated indefinitely, so long as the sample channel is not completely blocked by crystals, and can thus be flushed with KCl flows.

B. Permeability properties

To examine HMMs with different polymer network densities (Fig. 4), we photopolymerized HMMs from different precursor solutions within a single, three-channel device: the left HMM using a 50% v/v PEG-DA solution and the right HMM from the standard 20% v/v solution.
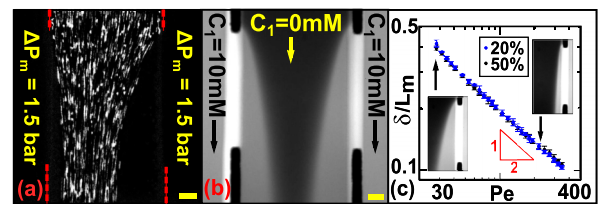

FIG. 4. (a) In the three-channel device [Figs. 1(b), 1(c), and 2], the amount of convection admitted by HMMs at large transmembrane pressure drops, here $\Delta P_m = 1.5$ bar, is lower for a highly cross-linked HMM (50% v/v, left) than for a lightly cross-linked HMM (20%, right). Tracer particles are focused towards the center of the channel by transmembrane flow from the side channels. (b) The diffusive flux through a lightly cross-linked membrane (20% v/v, right) is nearly identical to that through a highly cross-linked (50% v/v, left) membrane. (c) After diffusing through each HMM, the pH buffer is convected downstream, forming a boundary layer whose thickness decreases with Peclet number (flow velocity) like $Pe^{1/2}$, as expected for 2D convection-diffusion. Scale bars: 20 μm.

We first look at permeability to trans-HMM flow, which is undetectable (Fig. 2) under typical pressures (e.g., $\Delta P_m = 75$ mbar). Twentyfold higher trans-HMM pressures ($\Delta P_m = 1.5$ bar), however, drive trans-HMM flows strong enough to displace tracer particles by some distance δ_f from each wall [Fig. 4(a)]. A mass balance relates the fluid velocity $u_m^{L,R}$ through the left and right HMMs to the downstream particle-free widths $\delta_f^{L,M}$, and the maximum downstream tracer velocity u_{bot}, according to

$$u_m^{L,R} \approx 0.67 \frac{\delta_f^{L,R} u_{bot}}{L_m}, \qquad (1)$$

under the assumption that the downstream flow profile has developed to the standard Poiseuille flow profile [see the derivation in the Supplemental Material (SM) [62]; see also [63]]. Trans-HMM flows obey Darcy's law [64],

$$u_m = -\kappa \frac{\Delta P_m}{\eta w_m}, \qquad (2)$$

where η is the fluid viscosity and w_m is the membrane thickness. The Darcy permeability κ can be used to estimate the typical pore size $l_p \sim \sqrt{\kappa}$ [65], which is, in turn, set by the cross-link density and entanglement spacing (typically 3–8 nm for many polymers [66]). We found $\kappa^{L,R}$ for the left and right HMMs to be 4.4 and 11 nm^2, giving $l_p^{L,R} \sim 2$ and 3 nm for the 50% and 20% HMMs, respectively. We note that the pore size would change for different exposure times; the exposure times were selected as the minimum required for the solution to gel, which does not occur immediately, possibly because of an oxygen depletion time [57]. Larger exposure times result in wider, more diffuse gel membranes and smaller pores.

Despite the lower Darcy permeability of the 50% HMM, its diffusive flux is indistinguishable from that of the 20% HMM. In Fig. 4(b), both reservoir channels are buffered at pH 9.8 with 10-mM Na$_2$CO$_3$ and pressurized to 150 mbar, as done previously, whereas the sample channel is held at pH 6.3 by a 1-mM MES buffer. We set the flow velocity in the sample channel by controlling the hydrostatic pressure [67]. All solutions contain 25-μM fluorescein as a pH indicator, revealing a bright boundary layer alongside each HMM [Fig. 4(b)], with width δ defined when the intensity drops to 20% of its maximum value. Boundary layer widths for 20% and 50% HMMs are nearly identical at all channel velocities measured [Fig. 4(c)]. This indicates either identical effective diffusivity or solution-dominant mass transfer resistance for Na$_2$CO$_3$ in PEG-DA, since w_m is nearly identical for the two HMMs. Larger solutes, however, have been shown to have decreased diffusivity in high-concentration PEG-DA gels [47].

The shape of the boundary layer reflects the competing effects of diffusion and convection and thus depends upon the Peclet number Pe $= U w_s / D$, where U is the average velocity (calculated from the pressure head and hydraulic resistance [63]), w_s is the sample channel width, and D is the solute diffusivity (e.g., $D = 10^3$ μm^2/s for Na$_2$CO$_3$ [68]).

Depth-averaged "Hele-Shaw" flows in low-aspect ratio channels (here, 10 μm tall by 150 μm wide) have approximately uniform profiles. Solute diffusing perpendicular to such uniform flows at high Pe establishes boundary layers with thickness $\delta / w_s \sim$ Pe$^{-1/2}$, as observed here [Fig. 4(c)]. The detailed, three-dimensional concentration profile, however, will reflect the inhomogeneous (parabolic) flow across the channel [69].

V. RAPID DIALYSIS

We now describe HMM-rapid dialysis (HMM-RaD) experiments, in which HMMs are used to rapidly change a chemical microenvironment. We expect that HMM-RaD will enable a broad range of new studies in a variety of disciplines, with examples including provoking the responses of cells, embryos, organisms, and microbes to morphogens, chemokines, signaling proteins, drugs, or toxins [31]; modifying colloids and surfaces (e.g., for sample sorting, binding assays, or fundamental surface studies) [70]; and provoking the transient response of complex and soft materials [71].

We start with reversible HMM-RaD in a 150-μm-wide sample channel [Fig. 5(b) and related Video 4]. Fabrication
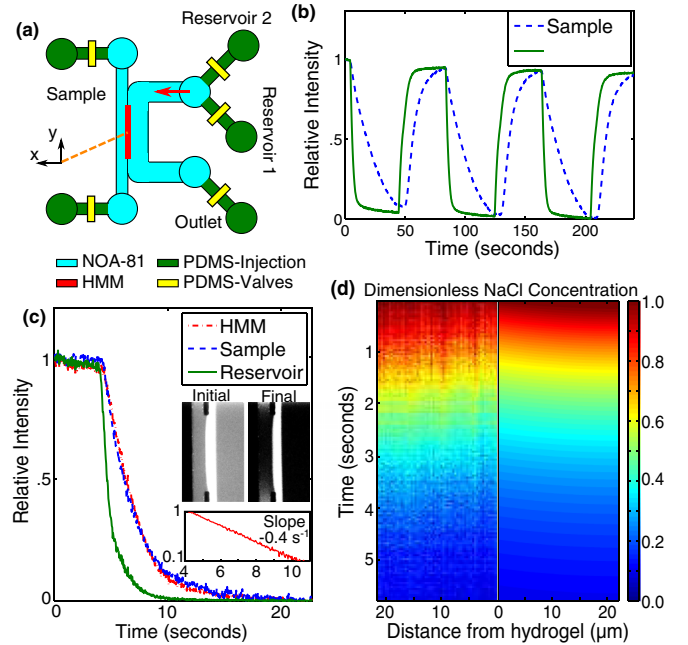

FIG. 5. (a) Device geometry for prompt reservoir solution swapping using PDMS valves and rapid dialysis in the sample channel using an HMM. Panel (b) and Video 4: Swapping between 250-mM-NaCl (bright) and 0-mM-NaCl (dark) solutions in a 150-μm-wide sample channel, with a fluorescent NaCl indicator. (c) Swapping time is greatly decreased by decreasing sample-channel width (here, 23 μm wide). Inset graph: Semilog plot of HMM intensity shows exponential decay of salt concentration in HMM. Panel (d) and Video 5: Observed dynamics of NaCl concentration along the x axis of the sample channel are well predicted by the one-dimensional diffusion equation.

details appear in Appendix A 2. NaCl was chosen as solute because of its relatively high diffusivity ($D = 1.6 \times 10^{-5}$ cm^2/s [68]) among salts with an available indicator dye (CoroNa Green, Invitrogen). Solutions were prepared consisting of 40-μM CoroNa Green, a 10-mM 3-(N-morpholino)propanesulfonic acid buffer (MOPS, pH 7), and 0-mM NaCl (dark) or 250-mM NaCl (bright). The fluorescence intensity of CoroNa was found to increase linearly with NaCl concentration in this range. Three 300-μm HMMs were polymerized to form a 900-μm-long HMM. The reservoir solutions were periodically switched every 40 seconds, and the relative fluorescence intensity $(I(t) - I_f)/(I_0 - I_f)$ was averaged over the sample channel region adjacent to the middle 300-μm HMM. The fluorescence intensity changes exponentially with a time scale $\tau_{\text{meas}} \approx 20$ s, which is slower than the $\tau_D = 7$ s predicted from simple diffusion through an inert HMM,

$$\tau_{\text{RaD}}^{\min} \sim \tau_D \sim \frac{4(w_m + w_s)^2}{\pi^2 D} \qquad (3)$$

(or, if solute was introduced from both sides and reservoirs synchronized, a factor of 4 faster). This result suggests that the HMM introduces a mass transport resistance comparable to that of the sample channel, discussed below.

By decreasing the width of the sample channel, even faster solution swapping could be performed (see Video 5). A HMM-RaD device with a sample channel of width $w_s = 23$ μm and a HMM of width $w_m = 17$ μm [for which Eq. (3) predicts $\tau_D = 0.4$ s] was fabricated for this purpose. Figure 5(c) shows the relative intensity averaged over the entire sample channel width and 1 μm of HMM at the sample interface. The intensity in the sample chamber closely follows that in the HMM, which changes exponentially with time constant $\tau_m = 2.5$ s. Swapping between 250 mM and 0 mM NaCl results in 90% NaCl removal in 5.6 seconds. Given the much faster τ_D from Eq. (3), the HMM-RaD is limited by the HMM itself. Figure 5(d) shows excellent agreement between the experimental concentration profile $c(x, t)$ and analytical theory within the sample chamber, imposing the experimentally observed τ_m as a boundary condition, but introducing no other free parameters (see the SM [62] for theoretical profile derivation; see also [72]). We anticipate that faster switching (of order τ_D) will be possible by optimizing HMM chemistry.

Several mass transport processes may lengthen the time required for HMM-RaD beyond Eq. (3): (i) diffusion across the boundary layer between the reservoir and the HMM (with resistivity $\Re_R \sim \delta_R/D$, where $\delta_R \sim \text{Pe}_R^{-1/2} L_m$), (ii) diffusion across the sample chamber ($\Re_s \sim w_s/D$), and (iii) diffusion through the HMM itself ($\Re_m \sim w_m/(D_m P)$). Here, P is the partition coefficient,

$$P = \frac{[C]_m}{[C]_s}, \qquad (4)$$

which expresses the ratio between equilibrium concentrations in the HMM and in the solution. The diffusivity D_m

may be slower within the HMM than in solution, with corrections due to lower porosity or mesh size that are often minor, or corrections that are more significant when the species adsorbs and desorbs from the gel. In addition to these steady-state mass transport limitations, highly partitioning solutes $P \gg 1$ require a finite time $\tau_C \sim P w_m C_s / j_D$ to "fill" the HMM, before even quasisteady diffusive permeation occurs.

VI. LOCAL ELECTRIC PERMEABILITY

Most microfluidic walls are electrically insulating, including NOA-81. The electric permeability of hydrogels, by contrast, suggests that HMMs may be used to sculpt electric fields in microfluidic systems, using electrodes in solutions that are physically distinct from the solution of interest.

To demonstrate the electrical behavior near HMMs, we electrophoretically oscillated 500-nm fluorescent polystyrene colloids [73] (Bangs Labs, FS03F) in a 1-mM NaCl solution in the sample channel of our standard three-channel device by imposing a 5-Hz, 400-V$_{pp}$, potential difference between stainless-steel pins at the inlets of the two reservoir channels. A 0.4-s exposure (Fig. 6) shows colloids tracing the local electric-field lines, much like iron filings in a magnetic field, confirming that the electric field passes through HMMs but not microchannel walls.

Integrating HMMs into electrode systems alleviates many issues that arise in conventional electrokinetic microfluidic systems. First, HMMs require no additional cleanroom processes, unlike photolithographically patterned electrodes, which require cleanroom metal deposition steps and separate masks. Second, electrochemical
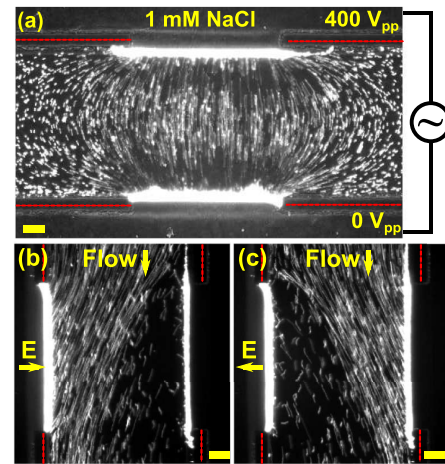

FIG. 6. (a) An ac potential applied between reservoir channel inlets drives an electric field that only crosses the sample channel through the HMMs. Fluorescent colloids in the sample channel oscillate electrophoretically, tracing local electric-field lines much like iron filings align with magnetic fields. Panels (b-c) and Video 6: Continuous-flow electrophoretic separations of negatively charged colloids by applying a dc electric field E transverse to the flow. Scale bars: 20 μm.

(Faradaic) reactions change solution composition near electrodes, e.g., generating gas bubbles or introducing gradients in pH or metal ions, potentially fouling nearby samples of interest. Instead, placing metal-pin electrodes in flowing electrolyte reservoirs behind HMMs allows undesirable electrochemical-reaction products or bubbles to be continually flushed away, thus maintaining steady electrolyte solutions and unfouled sample environments. No cleanroom time is required for the electrokinetic systems in Fig. 6, other than initial silicon master fabrication, although photopatterned electrodes could obviously be deposited onto channel floors using standard cleanroom techniques, if desired.

Figures 6(b) and 6(c) and related Video 6 show a continuous-flow particle separation enabled by HMMs. A dc field is applied across the HMMs, transverse to a pressure-driven flow, causing the flowing particles to move electrophoretically to one side of the channel. The direction of colloidal motion and downstream width-fraction containing colloids can be controlled by changing the voltage.

This ability to sculpt electric fields naturally suggests novel capabilities for a variety of experiments, including electrophoretic separations [74], local electrophoretic delivery [75], microfluidic salt bridges (e.g., for maintaining separate reference and working electrode solutions [76]), and localized or selective electroporation of cells, organisms, or vesicles [77]. While electrically permeable gels could also be made with contact lithography for these applications (and have been, in some cases [78–81]), HMMs enable closer electrode spacing, allowing higher currents and smaller dimensions to be obtained. With further development, HMM electrophoresis could be used for detection of changes in electrophoretic mobility (e.g., from binding of analyte) or cell sorting (cell separation based on an upstream measurement).

VII. LOCALIZED CONCENTRATION GRADIENTS

Steady microfluidic concentration gradients can be used to expose samples and surfaces to impose continuous concentration gradients across a sample, allowing high-throughput experiments (e.g., for optimization of reaction conditions, cellular response [82,83], or other concentration-dependent phenomena [84,85]). Chemical gradients also drive interesting and useful microscale phenomena such as diffusiophoresis [48,49,86–92], chemotaxis [46,93–95], and biological signaling [96–99].

The locally integratable nature of HMMs allows novel design capabilities for concentration fields, e.g., gradient shaping and integration into more complex chips without stringent demands on overall pressure balances. Multiple HMMs, each with its own distinct and individually addressable reservoir channel, enable the creation of almost arbitrarily complex chemical microenvironments composed of multiple species. The speed, ease, and small chip area of the HMMs makes them particularly appealing
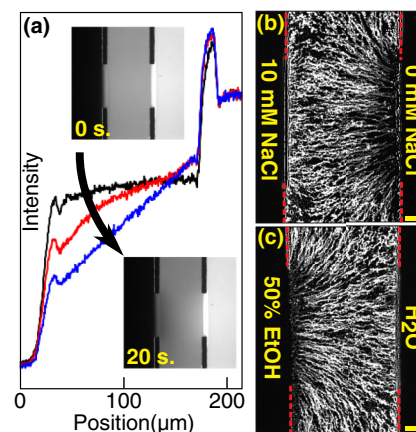

FIG. 7. Concentration gradients created locally within microchannels. (a) Direct gradient visualization with Oregon Green fluorescent dye at 0 (black), 10 (red), and 20 (blue) seconds after stopping flow. Panel (b) and Video 7: Diffusiophoretic motion of fluorescent colloids up a NaCl gradient. Panel (c) and Video 8: Solvophoretic motion down an ethanol gradient. Scale bar: 20 μm.

for producing on-chip concentration gradients, compared to other microfluidic methods.

Using our standard three-channel geometry, we apply HMMs to suddenly impose a fluorophore concentration gradient [Fig. 7(a)]. All three channels contain a 10-mM MES buffer, but each carries a different concentration of the fluorophore Oregon Green 488 (Invitrogen)—0 mM, 0.5 mM, and 1 mM, respectively—so that flowing channels appear dark, medium, and bright. Within several minutes of injecting these solutions, flow in the sample channel is quickly stopped using PDMS valves (0 s). A linear gradient is quickly established (20 s) and maintained at a steady state. The predicted diffusion time $[\tau_D = (2w_m + w_s)^2/(\pi^2 D) = 9$ s, based on $D = 4 \times 10^{-10}$ m^2/s [100]] agrees well with the transient time scale (i.e., $t \approx 2\tau_D$ for the transient to decay by 90%).

Solute gradients drive colloids into diffusiophoretic motion [Figs. 7(b) and 7(c)]. Nonetheless, it has been difficult to directly visualize colloidal diffusiophoresis, as concentration gradients strong enough to drive diffusiophoresis generally give rise to hydrodynamic instabilities in macroscopic experiments. By contrast, the small dimensions of microfluidic systems enable even strong gradients to remain hydrodynamically stable. Recent microfluidic experiments have visualized diffusio-electrophoresis in salt gradients [48,49,91,92]. Complementing these studies, here we demonstrate localized diffusio-electrophoresis along the sculpted gradients enabled by HMMs. Figure 7(b) and related Video 7 show the diffusiophoretic migration of colloids up a NaCl gradient established in a three-channel geometry ($\tau_D = 2.3$ sec). Channel solutions were initially established and maintained by flowing solutions of 10 mM NaCl (left reservoir), 5 mM NaCl with 500-nm polystyrene beads (sample), and DI water (right reservoir). Flow was quickly eliminated in the sample channel by submerging

both inlet tubes in a small beaker [101], and the following 8.3 s of fluorescence images were superposed. Beads clearly migrate diffusiophoretically up the gradient in NaCl, even tracking the two-dimensional (2D) "fringing" shape once the gradient is established.

HMMs can also be used to establish solvent gradients, which can drive colloidal diffusio-chemiophoresis [87,90] or "solvophoresis" [102]. While solvophoresis has been seen in macroscopic aggregation experiments [102], it has never been visualized experimentally. Exploiting the solvent compatibility of HMMs and NOA-81 devices, we show the first direct visualization of colloids moving solvophoretically [Fig. 7(c)].

To generate solvophoresis using HMMs, we start with flows of (left to right) 50%, 25%, and 0% v/v ethanol solutions in DI water ($\tau_D = 2.9$ s), with 10 mM KCl in each to balance ionic strength, and we superpose 10.4 s of images once the central flow is stopped. Polystyrene colloids migrate down the ethanol gradient solvophoretically [Fig. 7(c) and Video 8].

VIII. CONCLUSION

We have demonstrated a simple method for making thin (10–25-μm) hydrogel membranes that can be integrated into specified locations inside standard microchannels. HMMs enable exquisite control, in space and time, over local chemical microenvironments in microfluidic systems. Because of their high-diffusive and low-hydraulic permeability, reservoirs of constant composition can be established on one side of a HMM, driving diffusion of solute and solvent to the other side. Established techniques for microfluidic logic and flow control allow reservoirs to be switched quickly, resulting in rapid diffusive delivery to samples due to the short length scales typical in microfluidic systems. HMMs are permeable to a broad range of solutes and solvents, and their chemical or physical properties can be tuned for many applications. Integrating multiple HMMs, each with its own independently controlled reservoir channel, will enable strong gradients of multiple species to be imposed and, more broadly, spatiotemporal sculpting of local chemical microenvironments. Permeability of HMMs to electric fields opens avenues for electrokinetic studies and electrophoretic (rather than diffusive) delivery of solute.

We anticipate that this basic HMM strategy will enable a broad range of novel experimental capabilities in the science and engineering of physical, biological, chemical, medical, and material systems. To aid in adapting the HMMs for new applications, we note that the chemical and mechanical properties of the microwindow membranes themselves can be modified simply by adjusting the precursor solution composition, taking advantage of the versatile acrylate chemistry. One such method was described here, wherein the hydraulic permeability was decreased by increasing the PEG-DA precursor concentration. Other methods to tune hydrogel properties have appeared in the

flow lithography and UV-curable hydrogel literature, including enabling permeability to larger solutes (e.g., polymers, proteins, quantum dots), e.g., by introducing a porogen in the precursor solution [103] or novel photolithography techniques [104]; modifying hydrogel chemistry by polymerizing in the presence of other reactive molecules (e.g., acrylate-functionalized charged groups or receptors for specific ligands [105,106]), magnetic nanoparticles [107], or degradable components for controlled release [108]. Photopolymerizing within parallel laminar streams of distinct precursors [52] or in the presence of gradients [109,110] would generate anisotropic HMMs. Electrical conductivity of HMMs can be enhanced by photopolymerization of highly conductive polymers [79–81]. More generally, nearly any UV-curable solution can be patterned using this method, as long as the curing time is fast compared to the diffusion time for reactive species in the precursor solution (i.e., Dämkohler number $Da \gg 1$). Incorporating reactive species with lower diffusivities within the precursor solution may also decrease the HMM width.

New HMM applications and experiments will likely require new channel and membrane designs. Various photomask geometries could be used to make other HMM shapes, as long as uncured precursors can be flushed away or removed. The ultimate resolution of HMMs is set by the optical properties (e.g., depth of focus) of the microscope, as well as the optical wavelength used for photocuring. In particular, sharply defined HMM features can be attained within channels whose maximum height is no taller than the objective's depth of focus at a desired magnification [50,52]. To cross-link HMMs uniformly throughout taller channels (e.g., to accommodate larger samples), an increased depth of focus is required. This depth of focus can be attained with a lower magnification objective, but at the expense of HMM resolution in the sample plane. More complex, multiheight silicon masters could be fabricated to preserve this high resolution.

To conclude, hydrogel membrane microwindows provide exquisite control over microscale chemical transport, at low expense and with little fabrication time required. Few barriers exist for incorporating the technique in a wide variety of experiments, as they can be integrated into standard microfluidic devices, equipment, and techniques. The combination of simple fabrication, facile integration, versatile chemistry, independent control of multiple, noninterfering HMMs, and tight spatiotemporal control suggests broad impact across physics, chemistry, biology, and materials studies.

APPENDIX A: FABRICATION DETAILS

1. Standard HMM fabrication

Our standard HMM fabrication procedure (Fig. 1; see the SM [62] for details, with Refs. [9,10,60,67,111–113] therein) builds on recent techniques involving *in situ* photopolymerization of UV-curable hydrogels [52–56]. An aqueous hydrogel precursor solution was prepared using 20% v/v polyethylene glycol diacrylate (PEG-DA, $n = 400$, Polysciences Inc.), 2% v/v photoinitiator (2-hydroxy-2-methylpropiophenone, Sigma Aldrich), and silica tracer beads (1 mg/mL, Bangs Labs, 500 nm diameter). Just prior to use, this mixture was vortexed for 3 min; then, compressed air was bubbled through for 10 min to increase dissolved O_2 and prevent excess cross-linking. A photomask (a 60-μm-wide transparent slit in 1.5-cm-diameter transparency, CAD/Art Services) was inserted into the field stop of an inverted microscope (Nikon TE-2000U). Patterned UV light was magnified through a 20x extra-long working-distance (NA = 0.45) objective and aligned to the device and fluorescence camera (Andor iXon 885). Then, 10-μm-tall microchannels made of NOA-81 [60] were filled using a syringe connected to the central channel. The focus was adjusted to the center of the channel height. The flow was slowed to $\lesssim 10$ μm/s by adjusting the syringe pressure to balance any stray flows and viewing the resulting tracer-bead motion under phase contrast. Cross-linking was achieved using 550 ms of UV illumination from a mercury lamp (X-Cite 200DC, Lumen Dynamics) sent through a UV-filter cube (Nikon UV-2A, UV intensity after filtering: 30 mW/cm^2). Leak-free HMMs were verified by gently pressurizing the syringe and checking for bead motion on the other side of the membrane. If no leaks were found, the channels were promptly flushed with more precursor to prevent excess cross-linking. The cross-linking was repeated for each additional HMM. Precursor solution was then removed by flushing channels with DI water for several minutes.

To fabricate the higher-density HMM described in Sec. IV B, the same procedure was used, except the precursor solution contained 50% v/v PEG-DA and 5% v/v photoinitiator, and 110-ms exposure time was used.

2. HMM-rapid dialysis device fabrication

To investigate the temporal response of HMM-RaD experiments, we designed and fabricated trilayer devices [Fig. 5(a); see the SM [62] for the fabrication diagram]. The fluidic layer, cast in NOA-81, consisted of a sample channel (width w_s either 150 μm or 23 μm), separated from a reservoir channel (300 μm wide) by a HMM of width w_m of 17 μm. Solutions were delivered to the sample and reservoir channels through channels in a PDMS layer bonded atop the NOA-81 layer [112], and flows within the PDMS delivery channels were controlled with multilayer soft lithography "pushup" valves [10] at intersections of the control and injection channels. In order to rapidly change between two reservoir solutions, two valved injection channels met over the NOA-81 reservoir inlet; all other inlets had a single valved injection channel for eliminating flow. The single-layer NOA-81 device and two-layer PDMS device were fabricated separately according to standard "stickers" [60] and multilayer-soft-lithography [9] protocols, respectively, then ozone-bonded together. To achieve precise valve timing, PDMS control channels were filled from sealed fluid containers, which were switched between 0 and 750 mbar using computer-controlled solenoid valves (Pneumadyne S10MM-30-12-3) [9], while the two reservoir solutions were pressurized to 250 mbar.

---

[1] Ivar Meyvantsson and David J. Beebe, *Cell Culture Models in Microfluidic Systems*, Annu. Rev. Anal. Chem. **1**, 423 (2008).

[2] Aaron R. Wheeler, William R. Throndset, Rebecca J. Whelan, Andrew M. Leach, Richard N. Zare, Yish Hann Liao, Kevin Farrell, Ian D. Manger, and Antoine Daridon, *Microfluidic Device for Single-Cell Analysis*, Anal. Chem. **75**, 3581 (2003).

[3] Matthew M. Crane, Kwanghun Chung, Jeffrey Stirman, and Hang Lu, *Microfluidics-Enabled Phenotyping, Imaging, and Screening of Multicellular Organisms*, Lab Chip **10**, 1509 (2010).

[4] Petra S. Dittrich and Andreas Manz, *Lab-on-a-Chip: Microfluidics in Drug Discovery*, Nat. Rev. Drug Discov. **5**, 210 (2006).

[5] Jai Il Park, Amir Saffari, Sandeep Kumar, Axel Gnther, and Eugenia Kumacheva, *Microfluidic Synthesis of Polymer and Inorganic Particulate Materials*, Annu. Rev. Mater. Res. **40**, 415 (2010).

[6] T. M. Squires and S. R. Quake, *Microfluidics: Fluid Physics at the Nanoliter Scale*, Rev. Mod. Phys. **77**, 977 (2005).

[7] George M. Whitesides, *The Origins and the Future of Microfluidics*, Nature (London) **442**, 368 (2006).

[8] Todd Thorsen, Sebastian J. Maerkl, and Stephen R. Quake, *Microfluidic Large-Scale Integration.*, Science **298**, 580 (2002).

[9] J. Melin and S. R. Quake, *Microfluidic Large-Scale Integration: The Evolution of Design Rules for Biological Automation*, Annu. Rev. Biophys. Biomol. Struct. **36**, 213 (2007).

[10] M. A. Unger, H. P. Chou, T. Thorsen, A. Scherer, and S. R. Quake, *Monolithic Microfabricated Valves and Pumps by Multilayer Soft Lithography*, Science **288**, 113 (2000).

[11] M. Morel, J.C. Galas, M. Dahan, and V. Studer, *Concentration Landscape Generators for Shear Free Dynamic Chemical Stimulation*, Lab Chip **12,** 1340 (2012).

[12] Andrew Evan Kamholz, Bernhard H. Weigl, Bruce A. Finlayson, and Paul Yager, *Quantitative Analysis of Molecular Interaction in a Microfluidic Channel: The T-Sensor*, Anal. Chem. **71,** 5340 (1999).

[13] P. Hersen, M.N. McClean, L. Mahadevan, and S. Ramanathan, *Signal Processing by the HOG MAP Kinase Pathway*, Proc. Natl. Acad. Sci. U.S.A. **105,** 7165 (2008).

[14] Daniel Ahmed, Chung Yu Chan, Sz-Chin Steven Lin, Hari S. Muddana, Nitesh Nama, Stephen J. Benkovic, and Tony Jun Huang, *Tunable, Pulsatile Chemical Gradient Generation via Acoustically Driven Oscillating Bubbles*, Lab Chip **13,** 328 (2013).

[15] Noo Li Jeon, Stephan K.W. Dertinger, Daniel T. Chiu, Insung S. Choi, Abraham D. Stroock, and George M. Whitesides, *Generation of Solution and Surface Gradients Using Microfluidic Systems*, Langmuir **16,** 8311 (2000).

[16] Namhyun Choi, Kangsun Lee, Dong Woo Lim, Eun Kyu Lee, Soo-Ik Chang, Kwang W. Oh, and Jaebum Choo, *Simultaneous Detection of Duplex DNA Oligonucleotides Using a SERS-Based Micro-Network Gradient Chip*, Lab Chip **12,** 5160 (2012).

[17] Jules J. VanDersarl, Alexander M. Xu, and Nicholas A. Melosh., *Rapid Spatial and Temporal Controlled Signal Delivery over Large Cell Culture Areas*, Lab Chip **11,** 3057 (2011).

[18] H.P. Chou, M.A. Unger, and S.R. Quake, *A Microfabricated Rotary Pump*, Biomed. Microdevices **3,** 323 (2001).

[19] Carl L. Hansen, Morten O.A. Sommer, and Stephen R. Quake, *Systematic Investigation of Protein Phase Behavior with a Microfluidic Formulator*, Proc. Natl. Acad. Sci. U.S.A. **101,** 14431 (2004).

[20] F.K. Balagaddé, L. You, C.L. Hansen, F.H. Arnold, and S.R. Quake, *Long-Term Monitoring of Bacteria Undergoing Programmed Population Control in a Microchemostat*, Science **309,** 137 (2005).

[21] Carl Hansen and Stephen R Quake, *Microfluidics in Structural Biology: Smaller, Faster Better*, Curr. Opin. Struct. Biol. **13,** 538 (2003).

[22] C.L. Hansen, S. Classen, J.M. Berger, and R. Stephen, *A Microfluidic Device for Kinetic Optimization of Protein Crystallization and In Situ Structure Determination*, J. Am. Chem. Soc. **128,** 3142 (2006).

[23] Sarah L. Perry, Griffin W. Roberts, Joshua D. Tice, Robert B. Gennis, and Paul J.A. Kenis, *Microfluidic Generation of Lipidic Mesophases for Membrane Protein Crystallization*, Cryst. Growth Des. **9,** 2566 (2009).

[24] Aaron M. Streets and Stephen R. Quake, *Ostwald Ripening of Clusters During Protein Crystallization*, Phys. Rev. Lett. **104,** 178 (2010).

[25] Wenbin Du, Liang Li, Kevin P. Nichols, and Rustem F. Ismagilov, *SlipChip*, Lab Chip **9,** 2286 (2009).

[26] Liang Li and Rustem F. Ismagilov, *Protein Crystallization Using Microfluidic Technologies Based on Valves, Droplets, and Slipchip*, Annu. Rev. Biophys. **39,** 139 (2010).

[27] Liang Li, Wenbin Du, and Rustem F. Ismagilov, *Multiparameter Screening on Slipchip Used for Nanoliter Protein Crystallization Combining Free Interface Diffusion and Microbatch Methods*, J. Am. Chem. Soc. **132,** 112 (2010).

[28] Tino Frank and Savaş Tay, *Flow-Switching Allows Independently Programmable, Extremely Stable, High-Throughput Diffusion-Based Gradients*, Lab Chip **13,** 1273 (2013).

[29] Javier Atencia, Jayne Morrow, and Laurie E. Locascio, *The Microfluidic Palette: A Diffusive Gradient Generator with Spatio-Temporal Control*, Lab Chip **9,** 2707 (2009).

[30] J. De Jong, R.G.H. Lammertink, and M. Wessling, *Membranes and Microfluidics: A Review*, Lab Chip **6,** 1125 (2006).

[31] Thomas M. Keenan and Albert Folch, *Biomolecular Gradients in Cell Culture Systems*, Lab Chip **8,** 34 (2007).

[32] David J. Beebe, Jeffrey S. Moore, Joseph M. Bauer, Qing Yu, Robin H. Liu, Chelladurai Devadoss, and Byung-Ho Jo, *Functional Hydrogel Structures for Autonomous Flow Control Inside Microfluidic Channels*, Nature (London) **404,** 588 (2000).

[33] Wei Zhan, Gi Hun Seong, and Richard M. Crooks, *Hydrogel-Based Microreactors as a Functional Component of Microfluidic Systems*, Anal. Chem. **74,** 4647 (2002).

[34] G.H. Seong, W. Zhan, and R.M. Crooks, *Fabrication of Microchambers Defined by Photopolymerized Hydrogels and Weirs within Microfluidic Systems: Application to DNA Hybridization*, Anal. Chem. **74,** 3372 (2002).

[35] A.E. Herr and A.K. Singh, *Photopolymerized Cross-Linked Polyacrylamide Gels for on-Chip Protein Sizing*, Anal. Chem. **76,** 4727 (2004).

[36] Darren Cherng-Wen Tan, Lin-Yue Lanry Yung, and Partha Roy, *Controlled Microscale Diffusion Gradients in Quiescent Extracellular Fluid*, Biomed. Microdevices **12,** 523 (2010).

[37] Augusto M Tentori and Amy E Herr., *Photopatterned Materials in Bioanalytical Microfluidic Technology*, J. Micromech. Microeng. **21,** 054001 (2011).

[38] Simon Song, Anup K. Singh, Timothy J. Shepodd, and Brian J. Kirby, *Microchip Dialysis of Proteins Using In Situ Photopatterned Nanoporous Polymer Membranes*, Anal. Chem. **76,** 2367 (2004).

[39] Simon Song, Anup K. Singh, and Brian J. Kirby, *Electrophoretic Concentration of Proteins at Laser-Patterned Nanoporous Membranes in Microchips*, Anal. Chem. **76,** 4589 (2004).

[40] Anson V. Hatch, Amy E. Herr, Daniel J. Throckmorton, James S. Brennan, and Anup K. Singh, *Integrated Preconcentration SDSPAGE of Proteins in Microchips Using Photopatterned Cross-Linked Polyacrylamide Gels*, Anal. Chem. **78,** 4976 (2006).

[41] Dongshin Kim and David J. Beebe, *Interfacial Formation of Porous Membranes with Poly (Ethylene Glycol) in a Microfluidic Environment*, J. Appl. Polym. Sci. **110,** 1581 (2008).

[42] Eunpyo Choi, Hyung-kwan Chang, Chae Young Lim, Taesung Kim, and Jungyul Park, *Concentration Gradient Generation of Multiple Chemicals Using Spatially Controlled Self-Assembly of Particles in Microchannels*, Lab Chip **12,** 3968 (2012).

[43] Tzu-Chi Kuo, Cannon, Yanning Chen, Joseph J. Tulock, Mark A. Shannon, Jonathan V. Sweedler, and Paul W. Bohn, *Gateable Nanofluidic Interconnects for Multilayered Microfluidic Separation Systems*, Anal. Chem. **75**, 1861 (2003).

[44] Chorong Kim, Kristina Kreppenhofer, Jubin Kashef, Dietmar Gradl, Dirk Herrmann, Marc Schneider, Ralf Ahrens, Andreas Guber, and Doris Wedlich, *Diffusion- and Convection-Based Activation of Wnt/β-Catenin Signaling in a Gradient Generating Microfluidic Chip*, Lab Chip **12**, 5186 (2012).

[45] Benjamin P. Casavant, Erwin Berthier, Ashleigh B. Theberge, Jean Berthier, Sara I. Montanez-Sauri, Lauren L. Bischel, Kenneth Brakke, Curtis J. Hedman, Wade Bushman, and Nancy P. Keller, *Suspended Microfluidics*, Proc. Natl. Acad. Sci. U.S.A. **110**, 10111, 2013.

[46] Shing-Yi Cheng, Steven Heilman, Max Wasserman, Shivaun Archer, Michael L. Shuler, and Mingming Wu, *A Hydrogel-Based Microfluidic Device for the Studies of Directed Cell Migration*, Lab Chip **7**, 763 (2007).

[47] Michael P. Cuchiara, Alicia C. B. Allen, Theodore M. Chen, Jordan S. Miller, and Jennifer L. West, *Multilayer Microfluidic PEGDA Hydrogels*, Biomaterials **31**, 5491 (2010).

[48] Jérémie Palacci, Benjamin Abécassis, Cécile Cottin-Bizonne, Christophe Ybert, and Lydéric Bocquet, *Colloidal Motility and Pattern Formation Under Rectified Diffusiophoresis*, Phys. Rev. Lett. **104**, 138 (2010).

[49] Jérémie Palacci, Cécile Cottin-Bizonne, Christophe Ybert, and Lydéric Bocquet, *Osmotic Traps for Colloids and Macromolecules Based on Logarithmic Sensing in Salt Taxis*, Soft Matter **8**, 980 (2012).

[50] J. C. Love, D. B. Wolfe, H. O. Jacobs, and G. M. Whitesides, *Microscope Projection Photolithography for Rapid Prototyping of Masters with Micron-Scale Features for Use in Soft Lithography*, Langmuir **17**, 6005 (2001).

[51] Dhananjay Dendukuri, Kim Tsoi, T. Alan Hatton, and Patrick S. Doyle, *Controlled Synthesis of Nonspherical Microparticles Using Microfluidics*, Langmuir **21**, 2113 (2005).

[52] Dhananjay Dendukuri, Daniel C. Pregibon, Jesse Collins, T. Alan Hatton, and Patrick S. Doyle, *Continuous-Flow Lithography for High-Throughput Microparticle Synthesis*, Nat. Mater. **5**, 365 (2006).

[53] Dhananjay Dendukuri, Shelley S. Gu, Daniel C. Pregibon, T. Alan Hatton, and Patrick S. Doyle, *Stop-Flow Lithography in a Microfluidic Device*, Lab Chip **7**, 818 (2007).

[54] Priyadarshi Panda, Shamsher Ali, Edward Lo, Bong Geun Chung, T. Alan Hatton, Ali Khademhosseini, and Patrick S. Doyle, *Stop-Flow Lithography to Generate Cell-Laden Microgel Particles*, Lab Chip **8**, 1056 (2008).

[55] Robert F. Shepherd, Priyadarshi Panda, Zhihao Bao, Kenneth H. Sandhage, T. Alan Hatton, Jennifer A. Lewis, and Patrick S. Doyle, *Stop-Flow Lithography of Colloidal, Glass, and Silicon Microcomponents*, Adv. Mater. **20**, 4734 (2008).

[56] Matthew E. Helgeson, Stephen C. Chapin, and Patrick S. Doyle, *Hydrogel Microparticles from Lithographic Processes: Novel Materials for Fundamental and Applied Colloid Science*, Curr. Opin. Colloid Interface Sci. **16**, 106 (2011).

[57] Dhananjay Dendukuri, Priyadarshi Panda, Ramin Haghgooie, Ju Min Kim, T. Alan Hatton, and Patrick S. Doyle, *Modeling of Oxygen-Inhibited Free Radical Photopolymerization in a PDMS Microfluidic Device*, Macromolecules **41**, 8547 (2008).

[58] C. Randall, Kelly M. Schultz, and Patrick S. Doyle, *Methods to Electrophoretically Stretch DNA: Microcontractions, Gels, and Hybrid Gel-Microcontraction Devices*, Lab Chip **6**, 516 (2006).

[59] J. Liu, D. Gao, H. F. Li, and J. M. Lin. *Controlled Photopolymerization of Hydrogel Microstructures inside Microchannels for Bioassays*, Lab Chip **9**, 1301 (2009).

[60] D. Bartolo, G. Degré, P. Nghe, and V. Studer, *Microfluidic Stickers*, Lab Chip **8**, 274 (2008).

[61] Charles E. Hoyle and Christopher N. Bowman, *ThiolEne Click Chemistry*, Angew. Chem., Int. Ed. Engl. **49**, 1540 (2010).

[62] See Supplemental Material at http://link.aps.org/supplemental/10.1103/PhysRevX.3.041010 for detailed derivations and experimental methods.

[63] H. Bruus, *Theoretical Microfluidics* (Oxford University Press, New York, 2007), Vol. 18.

[64] L. G. Leal, *Advanced Transport Phenomena: Fluid Mechanics and Convective Transport Processes* (Cambridge University Press, Cambridge, England, 2007).

[65] Kristin J. Mattern, Chalida Nakornchai, and William M. Deen, *Darcy Permeability of Agarose-Glycosaminoglycan Gels Analyzed Using Fiber-Mixture and Donnan Models*, Biophys. J. **95**, 648(2008).

[66] P. C. Hiemenz and T. P. Lodge, *Polymer Chemistry* (CRC Press, Boca Raton, 2007), 2nd ed.

[67] Alex Groisman, Markus Enzelberger, and Stephen R. Quake, *Microfluidic Memory and Control Devices*, Science **300**, 955 (2003).

[68] E. L. Cussler, *Diffusion: Mass Transfer in Fluid Systems* (Cambridge University Press, Cambridge, England, 1997).

[69] Rustem F. Ismagilov, Abraham D. Stroock, Paul J. A. Kenis, George Whitesides, and Howard A. Stone, *Experimental and Theoretical Scaling Laws for Transverse Diffusive Broadening in Two-Phase Laminar Flows in Microchannels*, Appl. Phys. Lett. **76**, 2376 (2000).

[70] R. A. Sperling and W. J. Parak, *Surface Modification, Functionalization and Bioconjugation of Colloidal Inorganic Nanoparticles*, Phil. Trans. R. Soc. A **368**, 1333 (2010).

[71] Jan Scrimgeour, Jae Kyu Cho, Victor Breedveld, and Jennifer Curtis, *Microfluidic Dialysis Cell for Characterization of Macromolecule Interactions*, Soft Matter **7**, 4762 (2011).

[72] Stanley J. Farlow, *Partial Differential Equations for Scientists and Engineers* (Dover Publications, New York, 1993).

[73] M. H. Oddy and J. G. Santiago, *A Method for Determining Electrophoretic and Electroosmotic Mobilities Using AC and DC Electric Field Particle Displacements*, J. Colloid Interface Sci. **269**, 192 (2004).

[74] Toru Takahashi, Sachiko Ogata, Matsuhiko Nishizawa, and Tomokazu Matsue, *A Valveless Switch for Microparticle Sorting with Laminar Flow Streams and Electrophoresis Perpendicular to the Direction of Fluid Stream*, Electrochem. Comm. **5**, 175 (2003).

[75] Allan S. Hoffman, *Hydrogels for Biomedical Applications*, Adv. Drug Delivery Rev. **64**, 18 (2012).

[76] E. Victoria Dydek, Montana V. Petersen, Daniel G. Nocera, and Klavs F. Jensen, *Realization of a Salt Bridge-Free Microfluidic Reference Electrode*, Lab Chip **12**, 1431 (2012).

[77] M. B. Fox, D. C. Esveld, A. Valero, R. Luttge, H. C. Mastwijk, P. V. Bartels, A. Van Den Berg, and R. M. Boom, *Electroporation of Cells in Microfluidic Devices: A Review*, Anal. Bioanal. Chem. **385**, 474 (2006).

[78] Rahul Dhopeshwarkar, Li Sun, and Richard M. Crooks, *Electrokinetic Concentration Enrichment within a Microfluidic Device Using a Hydrogel Microplug*, Lab Chip **5**, 1148 (2005).

[79] Honggu Chun, Taek Dong Chung, and Hee Chan Kim, *Cytometry and Velocimetry on a Microfluidic Chip Using Polyelectrolytic Salt Bridges*, Anal. Chem. **77**, 2490 (2005).

[80] Kwang Bok Kim, Honggu Chun, Hee Chan Kim, and Taek Dong Chung, *Red Blood Cell Quantification Microfluidic Chip Using Polyelectrolytic Gel Electrodes*, Electrophoresis **30**, 1464 (2009).

[81] Honggu Chun, Taek Dong Chung, and J. Michael Ramsey, *High Yield Sample Preconcentration Using a Highly Ion-Conductive Charge-Selective Polymer*, Anal. Chem. **82**, 6287 (2010).

[82] Serge Ostrovidov, Nasim Annabi, Azadeh Seidi, Murugan Ramalingam, Fariba Dehghani, Hirokazu Kaji, and Ali Khademhosseini, *Controlled Release of Drugs from Gradient Hydrogels for High-Throughput Analysis of CellDrug Interactions*, Anal. Chem. **84**, 1302 (2012).

[83] Chandrasekhar R. Kothapalli, Ed van Veen, Sarra de Valence, Seok Chung, Ioannis K. Zervantonakis, Frank B. Gertler, and Roger D. Kamm, *A High-Throughput Microfluidic Assay to Study Neurite Response to Growth Factor Gradients*, Lab Chip **11**, 497 (2011).

[84] Andrew J. Pascall and Todd M. Squires, *Induced Charge Electro-osmosis over Controllably Contaminated Electrodes*, Phys. Rev. Lett. **104**, 088 (2010).

[85] Andrew J. Pascall and Todd M. Squires, *An Automated, High-Throughput Experimental System for Induced Charge Electrokinetics*, Lab Chip **10**, 2350 (2010).

[86] B. V. Derjaguin, G. P. Sidorenkov, E. A. Zubashchenkov, and E. V. Kiseleva, *Kinetic Phenomena in Boundary Films of Liquids*, Kolloidn. Zh. **9**, 335 (1947).

[87] J. L. Anderson, M. E. Lowell, and D. C. Prieve *Motion of a Particle Generated by Chemical Gradients Part 1. Non-Electrolytes.*, J. Fluid Mech. **117**, 107 (1982).

[88] D. C. Prieve, J. L. Anderson, J. P. Ebel, and M. E. Lowell *Motion of a Particle Generated by Chemical Gradients. Part 2. Electrolytes.*, J. Fluid Mech. **148**, 247 (1984).

[89] J. P. Ebel, John L. Anderson, and D. C. Prieve, *Diffusiophoresis of Latex Particles in Electrolyte Gradients*, Langmuir **4**, 396 (1988).

[90] John L. Anderson, *Colloid Transport by Interfacial Forces*, Annu. Rev. Fluid Mech. **21**, 61 (1989).

[91] B. Abécassis, C. Cottin-Bizonne, C. Ybert, A. Ajdari, and L. Bocquet, *Boosting Migration of Large Particles by Solute Contrasts*, Nat. Mater. **7**, 785 (2008).

[92] B. Abécassis, C. Cottin-Bizonne, C. Ybert, A. Ajdari, and L. Bocquet, *Osmotic Manipulation of Particles for Microfluidic Applications*, New J. Phys. **11**, 075022 (2009).

[93] Dirk Dormann and Cornelis J. Weijer, *Chemotactic Cell Movement During Development*, Curr. Opin. Genet. Dev. **13**, 358 (2003).

[94] Jinpian Diao, Lincoln Young, Sue Kim, Elizabeth A. Fogarty, Steven M. Heilman, Peng Zhou, Michael L. Shuler, Mingming Wu, and Matthew P. DeLisa, *A Three-Channel Microfluidic Device for Generating Static Linear Gradients and Its Application to the Quantitative Analysis of Bacterial Chemotaxis*, Lab Chip **6**, 381 (2006).

[95] Daniel Irimia, *Microfluidic Technologies for Temporal Perturbations of Chemotaxis*, Annu. Rev. Biomed. Eng. **12**, 259 (2010).

[96] Carl Nathan, *Neutrophils and Immunity: Challenges and Opportunities*, Nat. Rev. Immunol. **6**, 173 (2006).

[97] Jason G. Cyster, *Chemokines and Cell Migration in Secondary Lymphoid Organs*, Science **286**, 2098 (1999).

[98] James B. Moseley, Adeline Mayeux, Anne Paoletti, and Paul Nurse, *A Spatial Gradient Coordinates Cell Size and Mitotic Entry in Fission Yeast*, Nature (London) **459**, 857 (2009).

[99] Julien Dubrulle and Olivier Pourquié, *fgf8 mRNA Decay Establishes a Gradient that Couples Axial Elongation to Patterning in the Vertebrate Embryo*, Nature (London) **427**, 419 (2004).

[100] C. B. Mller, A. Loman, V. Pacheco, F. Koberling, D. Willbold, W. Richtering, and J. Enderlein, *Precise Measurement of Diffusion by Multi-Color Dual-Focus Fluorescence Correlation Spectroscopy*, Europhys. Lett. **83**, 46001 (2008).

[101] Tobias S. Mansuripur, A. J. Pascall, and T. M. Squires, *Asymmetric Flows over Symmetric Surfaces: Capacitive Coupling in Induced-Charge Electro-osmosis*, New J. Phys. **11**, 075030 (2009).

[102] Marek Kosmulski and Egon Matuevi, *Solvophoresis of Latex*, J. Colloid Interface Sci. **150**, 291 (1992).

[103] Nak Won Choi, Jungwook Kim, Stephen C. Chapin, Thao Duong, Elaine Donohue, Pramod Pandey, Wendy Broom, W. Adam Hill, and Patrick S. Doyle, *Multiplexed Detection of mRNA Using Porosity-Tuned Hydrogel Microparticles*, Anal. Chem. **84**, 9370 (2012).

[104] Ji-Hyun Jang, Dhananjay Dendukuri, T. Alan Hatton, Edwin L. Thomas, and Patrick S. Doyle, *A Route to Three-Dimensional Structures in a Microfluidic Device: Stop-Flow Interference Lithography*, Angew. Chem. **119**, 9185 (2007).

[105] Daniel C. Pregibon, Mehmet Toner, and Patrick S. Doyle, *Multifunctional Encoded Particles for High-Throughput Biomolecule Analysis*, Science **315**, 1393 (2007).

[106] Rathi L. Srinivas, Stephen C. Chapin, and Patrick S. Doyle., *Aptamer-Functionalized Microgel Particles for Protein Detection*, Anal. Chem. **83**, 9138 (2011).

[107] Dae Kun Hwang, Dhananjay Dendukuri, and Patrick S. Doyle, *Microfluidic-Based Synthesis of Non-Spherical Magnetic Hydrogel Microparticles*, Lab Chip **8,** 1640 (2008).

[108] Dae Kun Hwang, John Oakey, Mehmet Toner, Jeffrey A. Arthur, Kristi S. Anseth, Sunyoung Lee, Adam Zeiger, Krystyn J. Van Vliet, and Patrick S. Doyle, *Stop-Flow Lithography for the Production of Shape-Evolving Degradable Microgel Particles*, J. Am. Chem. Soc. **131,** 4499 (2009).

[109] Greg J. Sommer, Anup K. Singh, and Anson V. Hatch, *On-Chip Isoelectric Focusing Using Photopolymerized Immobilized pH Gradients*, Anal. Chem. **80,** 3327 (2008).

[110] Francesco Piraino, Gulden Camci-Unal, Matthew J. Hancock, Marco Rasponi, and Ali Khademhosseini, *Multi-Gradient Hydrogels Produced Layer by Layer with Capillary Flow and Crosslinking in Open Microchannels*, Lab Chip **12,** 659 (2012).

[111] Y. Xia and G. M. Whitesides, *Soft Lithography*, Annu. Rev. Mater. Sci. **28,** 153 (1998).

[112] J. C. Galas, D. Bartolo, and V. Studer, *Active Connectors for Microfluidic Drops on Demand*, New J. Phys. **11,** 075027 (2009).

[113] Vincent Studer, Giao Hang, Anna Pandolfi, Michael Ortiz, W. French Anderson, and Stephen R. Quake, *Scaling Properties of a Low-Actuation Pressure Microfluidic Valve*, J. Appl. Phys. **95,** 393 (2004).